Experimentally supported control design for a direct drive robot

Proceedings of the 2002 IEEE International
Conference on Control Applications
September 18-20, 2002 • Glasgow, Scotland, U.K.

Experimentally Supported Control Design for a Direct Drive Robot

Dragan Kostić,[1] *Student Member, IEEE*, Bram de Jager,[2] and Maarten Steinbuch,[3] *Senior Member, IEEE*
Dynamics and Control Technology Group, Department of Mechanical Engineering,
Eindhoven University of Technology (TU/e), P.O. Box 513, 5600 MB Eindhoven, The Netherlands
Phone: +31 40 247 5730, Fax: +31 40 246 1418
[1]D.Kostic@tue.nl, [2]A.G.de.Jager@wfw.wtb.tue.nl, and [3]M.Steinbuch@tue.nl

***Abstract*—We promote the idea of an experimentally supported control design as a successful way to achieve accurate tracking of reference robot motions, under disturbance conditions and given the uncertainties arising from modeling errors. The H_∞ robust control theory is used for design of motion controllers. Potential of the theory is additionally enhanced by incorporating a disturbance-based control design cycle. Within each iterative cycle we experimentally evaluate effects of designed H_∞ controllers on a direct-drive robotic set-up. The controllers resulting from such iterative design are indeed specialized for this robot, but they significantly improve both performance and robustness against disturbances and modeling errors, as compared with conventional industrial motion controllers. Superior performance is experimentally demonstrated in both configuration (joint) and task (Cartesian) spaces of the robot.**

***Index Terms*—Application, Robotics, PD control, H_∞ robust control, Kalman observer, Disturbance modeling.**

I. INTRODUCTION

In industrial robotics there is always a challenge to speed-up motions of the robot-tip, preserving desired accuracy of trajectory tracking and robustness against disturbances and model uncertainties. Increasing demands on the performance of robot manipulators has led to the development of versatile tracking control approaches [1-7].

Because of their simplicity, standard industrial controllers (PD or PID) are widely used with various control methods. Their simple structure makes them attractive for practical implementation. Industrial experience shows a robustness of these controllers against disturbances, such as friction and load torques. Finally, the majority of industrial robot systems are equipped with high-gear transmission mechanisms and hence can be described by decoupled linear equations [8]. The standard controllers seem to be a natural choice for such linear plants. However, if high-quality performance of trajectory tracking is needed, the standard controllers may lead to unsatisfactory results. Articles [3,9] address conflicting influences of these controllers on low-frequent accuracy, system stability, and damping of high-frequency disturbances. The conventional controllers assume use of full state information, i.e., availability of both position and velocity coordinates. To avoid use of expensive tachometers, the velocity coordinate is determined either by digital processing of signals from incremental encoders, or from velocity observers [6,10]. Both approaches enable control of robot motions using only position measurements [5,6]. Velocity observers obtained via Kalman design may contribute to the better performance of the standard controllers [6,10]. Even enhanced with the Kalman filters, these controllers may hardly reach ultimate bounds of the performance and robustness in the controlled system. It is shown in [3] that use of lead-lag compensators results in a small increase of off-line tuning effort and on-line computational load, but the improvements in robot performance may be significant. Moreover, if no transmission is present between joint actuators and links, which is typical for direct-drive robots, the nonlinear link-couplings directly apply upon each actuator and deteriorate the standard independent joint controller considerably. Since our experimental set-up belongs to the class of the direct-drive robots [8,11], we are naturally interested in control methods that may provide high performance and robustness properties even for this challenging robot class.

In this paper we promote idea of the experimentally supported (ES) control design as a mean to achieve both desired performance and robustness against disturbances and model uncertainties. We believe that a controlled system can be pushed to the feasible limits of performance and robustness only if all noticeable plant peculiarities are recognized and taken into account in control design. Our control approach relies on the reasoning promoted in [9]. It has been established in industrial practice with optical storage systems, where high performance and robustness of motion control are essential objectives. In this paper we extend its application to nonlinear and much more demanding control plants – direct-drive robots. We certainly do not favor our approach as the ultimate solution, but we strongly advice it to anybody requiring advanced experimental behavior of industrial robots. Shortly, we achieve the desired performance and robustness properties via frequency-domain techniques. A computed-torque method enables a linear feedback control design, for which we readily have several candidates: a loop shaping, H_2, H_∞, μ-synthesis [9]. Here we use the H_∞-optimization, in particular, an H_∞ solution to the mixed-sensitivity problem (MSP) [12]. This technique is selected just as an illustration and it is certainly not the only option we have. On the other hand, it can be easily implemented using standard software [13], and it is quite applicable to the problem at hand. In a systematic way it determines optimal controllers ensuring robustness against model uncertainties and parasitic effects, e.g., unmodeled flexibilities apparent after application of the computed-torque law, quantization noise and time-delay. Simultaneously, it allows us to boost the performance, defined as accuracy of trajectory tracking, close to the feasible limits. The essential ingredient of ES approach is the iterative disturbance-based control design cycle with experiments [9].

In the next section we describe a direct-drive robot used for experimental comparison of the standard and the ES control designs. Section III explains decoupling of the robot dynamics and presents a solution to the motion control problem using the conventional controller enhanced with Kalman filter. In Section IV we identify peculiarities of the robot dynamics. We also sketch a solution to the MSP using the H_∞-optimization, incorporated into the disturbance-based control design iteration. Section V discusses experimental results in motion control obtained using the conventional and ES control designs. Final remarks are given at the end.

0-7803-7386-3/02/$17.00 © 2002 IEEE

II. EXPERIMENTAL SET-UP

The RRR robot, shown in Fig. 1, is an experimental facility for the research in motion control [8,11]. Its three revolute degrees of freedom (d.o.f.) are actuated by gearless brushless DC direct-drive motors. The actuators are Dynaserv DM-series servos with nominal torques of 60, 30 and 15 Nm, respectively. Each actuator has integrated incremental optical encoder having 655360 lines of resolution. Servos are driven by power amplifiers with built in current controllers. Both encoders and amplifiers are connected to a PC-based control system. This system consists of the MultiQ I/O board from Quanser Consulting (8×13 bits ADC, 8×12 bits DAC, 8 digital I/O, 6 encoder inputs, and 3 hardware timers), combined with a commercial soft real-time system Wincon from Quanser Consulting. It facilitates design of controllers in MATLAB/Simulink and their real-time implementation. The control system features a time delayed angular joint response to the given control input. For the sampling time of $T_s = 1\,\text{ms}$, there is a delay of $\delta = 2T_s$. Detailed description of this problem is given in Section IV. The joints have infinite range of motions, since the power and the sensor signals are transferred via sliprings. Due to insufficient stiffness in mounting the robot base to the floor, two modest resonances at 13 and 22 Hz are present at the base. Such parasitic effects practitioners often experience in industry. However, they can be successfully handled using the ES control design.

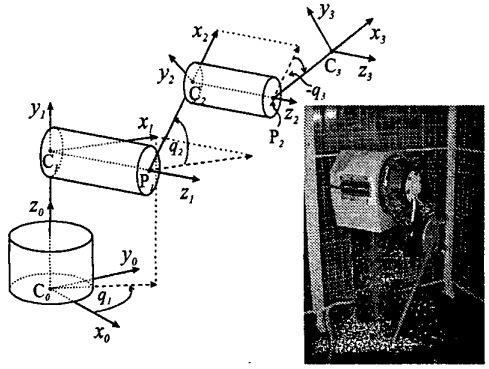

Fig. 1. Kinematic diagram and photo of the RRR robot

Models of the robot kinematics and dynamics are available in [14,15]. Their parameters are known with sufficient accuracy, allowing a real-time implementation of model-based control techniques. Using the kinematic model we may determine joint motions given a trajectory of the robot-tip. The rigid-body dynamic model has a form:

$$\boldsymbol{\tau}(t) = \mathbf{M}(\mathbf{q}(t))\ddot{\mathbf{q}}(t) + \mathbf{h}(\mathbf{q}(t), \dot{\mathbf{q}}(t)), \qquad (1)$$

where $\boldsymbol{\tau}$ is a 3×1 vector of control torques, $\mathbf{M}$ is a 3×3 inertia matrix, $\mathbf{q}$, $\dot{\mathbf{q}}$ and $\ddot{\mathbf{q}}$ are 3×1 vectors of joint motions, velocities and accelerations, respectively, and $\mathbf{h}$ is a 3×1 vector of Coriolis/centripetal, gravitational and friction effects. This model is used in the computed-torque control law:

$$\boldsymbol{\tau}_c(t) = \mathbf{M}(\mathbf{q}_{ref}(t))(\ddot{\mathbf{q}}_{ref}(t) + \mathbf{v}(t)) + \mathbf{h}(\mathbf{q}_{ref}(t), \dot{\mathbf{q}}_{ref}(t)), \qquad (2)$$

where '*ref*' stands for the reference motions, $\mathbf{v}$ is the linear feedback, and $\boldsymbol{\tau}_c$ is the total control law. Standard and ES control designs differ in the procedure how $\mathbf{v}$ is determined.

III. STANDARD CONTROL DESIGN

The PD controller is a conventional solution for industrial robots. When applied with the computer-torque method (2), it should ensure: (*i*) stability of robot motions, (*ii*) specified accuracy of trajectory tracking, and, (*iii*) robustness against disturbances (quantization noise, flexibilities) and model uncertainties caused by eventual mismatching between the model (1) and the real robot dynamics. The Bode plot of one PD controller is indicated in Fig. 2 with the stars. Its basic drawback is a poor reduction of disturbances at high frequencies. Quantization noise from the incremental encoders typically lies in this frequency range, and may be seriously amplified in the velocity loop of the PD. As a remedy, one may use a Kalman filter that reduces impact of the noise due to inherent low-pass filtering properties. Here we use a Kalman filter, which, in addition to the filtering effects, compensates for the time delay.

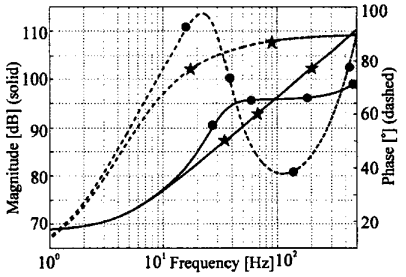

Fig. 2. PD controller without (stars) and with (circles) Kalman filter

After digital application of the control law (2) ($\boldsymbol{\tau}_c(t) = \boldsymbol{\tau}_c(k)$, k abbreviates kT_s), the robot dynamics reduces to

$$\left.\begin{aligned} \ddot{q}_i(k) &= \ddot{q}_{ref,i}(k) + v_i(k) + d_i(k) \\ \tilde{y}_i(k) &= q_i(k-2) \end{aligned}\right\} \; (i = 1,2,3). \qquad (3)$$

Variable d_i represents modeling errors in the case of imperfect compensation of the real robot dynamics using the model (1). In our experiments the standard assumption that d_i results from integration of the white process noise ς_i [10] is justified. Variable $\tilde{y}_i$ is the position measurement. Because of the time delay, the measurement at $t=kT_s$ is the joint angular response to the control input at $t=(k-2)T_s$.

In the design of the velocity observer, the position errors $e_i = q_i - q_{ref,i}$ (i=1,2,3) are regarded as the coordinates. By introducing the state-space notation, we may determine a discrete-time system having identical solutions with the model (3):

$$\left.\begin{aligned} \mathbf{x}_i(k+1) &= \mathbf{E}_i(T_s)\mathbf{x}_i(k) + \mathbf{f}_i(T_s)v_i(k) + \mathbf{g}_i(T_s)\varsigma_i(k) \\ y_i(k) &= \mathbf{c}_i\mathbf{x}_i(k) \end{aligned}\right\}, \qquad (4a)$$

where

$$\mathbf{x}_i(k) = [e_i(k-2),\, e_i(k-1), e_i(k), \dot{e}_i(k), d_i(k)]^T, \qquad (4b)$$

$$\mathbf{E}_i = \begin{bmatrix} 0 & 1 & 0 & 0 & 0 \\ 0 & 0 & 1 & 0 & 0 \\ 0 & 0 & 1 & T_s & T_s^2/2 \\ 0 & 0 & 0 & 1 & T_s \\ 0 & 0 & 0 & 0 & 1 \end{bmatrix}, \; \mathbf{f}_i = \begin{bmatrix} 0 \\ 0 \\ T_s^2/2 \\ T_s \\ 0 \end{bmatrix}, \; \mathbf{g}_i = \begin{bmatrix} 0 \\ 0 \\ T_s^3/6 \\ T_s^2/2 \\ T_s \end{bmatrix}, \qquad (4c)$$

$$\mathbf{c}_i = [1\;0\;0\;0\;0]. \qquad (4d)$$

Although not explicitly formulated in (4a), we assume that the output variable y_i is corrupted with measurement noise. A Kalman filter provides an optimal tradeoff between the model uncertainty (incorporated via ω_i) and the measurement noise:

$$\left.\begin{aligned}\hat{\mathbf{x}}_i(k+1) &= \mathbf{E}_i(T_s)\bar{\mathbf{x}}_i(k) + \mathbf{f}_i(T_s)v_i(k),\\ \bar{\mathbf{x}}_i(k) &= \hat{\mathbf{x}}_i(k) + \mathbf{k}_i(y_i(k) - \mathbf{c}_i\hat{\mathbf{x}}_i(k))\end{aligned}\right\}, \quad (5)$$

where $\bar{\mathbf{x}}_i$ denotes updated estimate of all states, y_i is the measured output of the system (4), and $\mathbf{k}_i$ is a 5×1 vector of constant Kalman gains. This filter predicts joint position and velocity errors at $t = kT_s$, from the known position error at $t = (k-2)T_s$. The prediction feature and inherent low-pass filtering characteristics recommends this filter as an enhancement of the PD controller. Practical effects of the PD with the Kalman filter, indicated in Fig. 2 with the circles, in the robot motion control, will be discussed in Section V.

IV. ES CONTROL DESIGN

When applied, the computed-torque control method (2) should decouple the robot dynamics. Problem of controlling the nonlinear-coupled system shifts to the problem of controlling the linear plants:

$$P_i(s) = q_i(s)/v_i(s) \ (i=1,2,3), \quad (6)$$

where s is the complex variable. Ideally, the plant transfer function P_i would be modeled as a single mass, i.e., a double integrator. Related frequency response function should have a linear amplitude plot with –2 slope and constant phase at –180° level. This holds if a perfectly rigid-body robot dynamics is completely linearized by the control law (2). In practice this may not happen. Rather than a double integrator, P_i has a more involved frequency response, incorporating peaks and zeros corresponding to resonance and anti-resonance frequencies. Location of these frequencies may vary in certain ranges as the robot changes its configuration. Such uncertainties in the real plant transfer function call for appropriate characterization. We should first determine a nominal model $P_{o,i}$ and then account for all structured and unstructured differences between the model and the measurements.

We will first explain procedures how to identify the nominal frequency response $P_{o,i}(j\omega)$ ($j=\sqrt{-1}$, ω-angular frequency), and the frequency response of the perturbed plant P_i (incorporates model variations). Identification experiment for the nominal model will be referred as of the *type I*. During it all the joints are allowed to move ($\dot{\mathbf{q}}_{ref}(t) \neq 0$). We use sinusoids with 180° amplitude and 4 s period as the joint references. Such sinusoids span the complete configuration space of the robot. Experiments to identify perturbed plants P_i are referred as of the *type II*. They are characterized by totally static robot configurations ($\dot{\mathbf{q}}_{ref}(t) \equiv 0$), or they allow a very slow, constant speed motion only for the joint whose P_i is identified. In our experiments the reference motion in the moving d.o.f. is a constant speed full revolution in one direction (duration 30 s) and identical revolution in the opposite direction. For both types of the identification experiments, the control law (2) is applied with:

$$\mathbf{v}(t) = -\mathbf{K}_p\mathbf{e}(t) - \mathbf{K}_d\dot{\mathbf{e}}(t) + \mathbf{n}(t), \quad (7)$$

where $\mathbf{K}_p = diag[k_{p,1}\ k_{p,2}\ k_{p,3}]$ and $\mathbf{K}_d = diag[k_{d,1}\ k_{d,2}\ k_{d,3}]$ are matrices of modest position and velocity gains, respectively. A 3×1 vector $\mathbf{n}$ contains a white noise excitation at the position i, corresponding to the d.o.f. whose $P_{o,i}$ or P_i is identified. As in the i-th identification experiment only $P_{o,i}$ or P_i is identified (to avoid undesirable interferences), other elements of $\mathbf{n}$ are identically zero. Our practical experience prefers the type I experiments when identifying $P_{o,i}$, as during them versatile peculiarities of robot dynamic behavior become better excited to be apparent from measurements. Since the type I experiments span the complete configuration space of the robot, the resulting frequency response is a kind of averaged responses one could get for static configurations (e.g., [0° 0° 0°], [0° 0° 90°], ..., [270° 270° 270°]). Differences between determined $P_{o,i}$ and P_i define model uncertainty.

High-accuracy in trajectory tracking and robustness against plant uncertainty and disturbances, can be successfully achieved using the controllers designed by H_∞ optimization, in particular, by reformulating the design problem as the MSP. The design method based on the mixed-sensitivity criterion features frequency response shaping, type k control and specified high-frequency roll-off, and direct control over the closed-loop bandwidth and time response by means of dominant pole placement. Denote a compensator acting as a feedback controller at i-th d.o.f. with C_i. The following transfer functions are well-known:

- Open-loop gain $L_i = P_iC_i$,
- Sensitivity function $S_i = 1/(1+L_i)$,
- Input sensitivity function $U_i = C_iS_i$.

As shown in [12], the problem of minimizing

$$\sqrt{\sup_{\omega\in R}\left(\left|W_{1,i}(j\omega)S_i(j\omega)\right|^2 + \left|W_{2,i}(j\omega)U_i(j\omega)\right|^2\right)} \quad (8)$$

with respect to all compensators C_i stabilizing a feedback loop with the gain L_i, is a version of the MSP. The function $W_{1,i}$ shapes S_i at low frequencies. It may force S_i to behave like ω^k as $\omega \to 0$ (type k control), ensuring a high reduction of position error within the bandwidth if $k \geq 1$. The weighting $W_{2,i}$ pre-assigns the high-frequency roll-off of U_i, and in turn of $P_iU_i = L_i/(1+L_i)$ (complementary sensitivity). The high-frequency roll-off reduces influence of disturbances at high frequencies.

The complete role of the weightings $W_{1,i}$ and $W_{2,i}$ has not been addressed, yet. In addition to the features explained above, we perform their fine-tuning in a disturbance-based control design cycle, with experiments within each cycle:

1. robot is moving along trajectories spanning the whole configuration space; a standard controller (as one indicated with stars in Fig. 2) is experimentally applied in the computed-torque control method (2), and *cumulative power spectrums* (CPS's – cumulative sums of power spectral densities over the whole frequency spectrum) of the measured position error and the control input are calculated; frequencies above the bandwidth of the joint references at which the CPS's have steeper slopes, reveal dynamic peculiarities (disturbances, flexibilities, noise) which should be tackled to achieve desired performance and robustness specifications,

2.the weightings $W_{1,i}$ and $W_{2,i}$ are tuned to account for the observed dynamic peculiarities,

3.optimal compensators C_i solving the MSP are computed and implemented on the robot,

4.CPS's of newly measured position errors and control inputs are calculated and evaluated; if the design specifications have not been met yet, the weightings $W_{1,i}$ and $W_{2,i}$ are adjusted again,

5.the steps 3 and 4 are repeated until further improvement of the performance can not be achieved.

Effectiveness of this iterative design will be presented next.

V. Experimental Evaluation

Design for performance and robustness is demonstrated on the robot's 1st d.o.f. Identical procedures hold for the other joints. The frequency response for this d.o.f., depicted in Fig. 3 with the solid line, is determined via the type I identification experiment. Position is directly taken from the incremental encoders. Expected dynamics is that of the double integrator (see Section IV). Practically, the frequency response of the considered d.o.f. is more involved. From the given plots we may immediately notice modest resonances around 13 and 22 Hz, and two profound resonances around 95 and 410 Hz. The modest resonances are due to insufficient stiffness in mounting the robot base to the floor. Being inherently accompanied with a temporary phase lead (see phase plot in Fig. 3), they are not a problem for the stability of motion. However, they may deviate position of the robot tip and in turn spoil the robot performance in the task space. Although by better mounting of the base we may suppress its parasitic vibrations, in this paper we will use the control design as a remedy. In that way we want to demonstrate advanced capabilities of the control design we promote here. We are also focused on reducing the impact from the profound resonances around 95 and 410 Hz, both in terms of extension of the possible closed-loop bandwidth, and in terms of robustness against variations in damping and location (frequency) of these resonances. By suppressing them, we will reduce influence of other disturbances belonging to the compatible frequency ranges (e.g., noise). Another problem to be solved by the control is the time-delay δ, addressed in Section II. If the phase diagram shown in Fig. 4 is plotted linearly with respect to the frequency, a linear decrease in phase of 360° will be visible after 500 Hz. As such phase lag can be described as $-360^\circ \delta f$, where δ is the time-delay and f is frequency in [Hz], it follows that $\delta = 1/500 = 2$ ms, which is exactly equal to $2T_s$. The same time delay is present in the other two d.o.f.

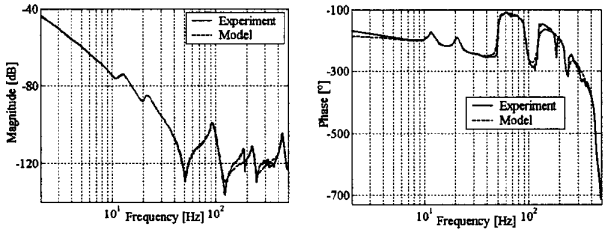

Fig. 3. Measured and identified plant models for the 1st d.o.f.

The conventional feedback controllers (without and with the Kalman filter) are designed according to the theory presented in Section III. The controllers' gains are determined such to provide stability with the largest possible closed-loop bandwidth, high open-loop gain within the bandwidth, and maximum peaking in the sensitivity function of 6 dB [9]. Additional filters for achieving the high-frequency roll-off are not engaged, as conventional robotic literature rarely addresses such option. Commonly, control engineers in the robotics just (naively?) rely on the low-pass filtering characteristics of the state observers. The open-loop gains for the feedback loop in the 1st d.o.f., obtained with the PD controllers shown in Fig. 2, are depicted in Fig. 4. The plots for the sole PD controller, depicted with the dotted lines, reveal small open-loop gain within the bandwidth and poor effects on reducing the resonances. By inspection of the plots depicted with the solid lines we see that even use of the Kalman filter may have limited effect on reducing the impact of the resonances, and in turn of the parasitic effects from the compatible frequency ranges. The PD controller enhanced with the filter succeeds only in damping the resonance around 410 Hz. It has just moderate influence on the resonance around 95 Hz, since it provides the magnitude peak just below the level as with the PD solely. Being insufficiently reduced, both resonances are manifested as peaks in the sensitivity functions plotted in Fig. 5. Controllers in the other two joints are designed in the same fashion and they feature the similar weaknesses.

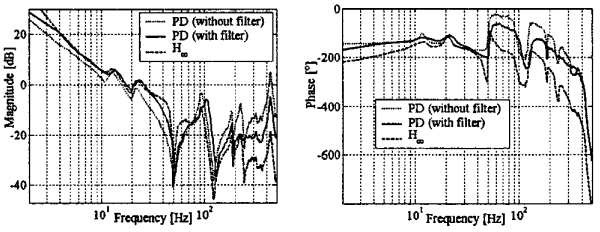

Figs 4. Experimental open-loop gains for the 1st d.o.f.

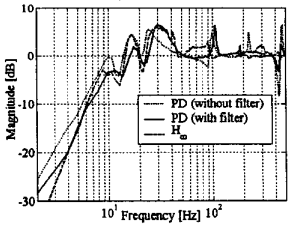

Fig. 5. Experimental sensitivity functions for the 1st d.o.f.

The quality of the controllers is evaluated in a very demanding motion task, defined in the joint space. The joints should perform fast displacements of 180° (duration 1 s), each time in opposite direction. The position references and the corresponding velocity profile are presented on the left in Fig. 6. The movements are demanding, as during each period of displacement the joint actuators almost reach their maximal torque levels. The position errors obtained using the PD with the filter are presented on the right in Fig. 6 with the gray lines. Having in mind the resolution of the position sensors (see Section II), it is clear that the achieved tracking errors are not satisfactory. Because of the lower open-loop gains within the bandwidth, the effect of the simple PD's are even worse and hence there is no need to be presented. In Fig. 7 we show the CPS's of the 1st error (left) and of the control input to the 1st motor (right) for both the PD (dotted) and for the PD with filter (solid). Note that the CPS of the position error, achieved using the sole PD, uses a larger scale, seen on the right vertical axis. We may observe from the given plots

that most of the signals' energy lies within the bandwidth of the joint references (up to 5 Hz). This reveals insufficient reduction of the position errors within the bandwidth. We see that above the bandwidth, both CPS's for the tracking errors do not dramatically change their slopes. It seems that the conventional controllers provide robust trajectory tracking even in the presence of the resonance frequencies. Unfortunately, the sole PD controller establishes such situation for the price of the chattering effects in the control input. The control input chatters exactly at the two previously recognized resonance frequencies, as obvious from the dotted plot on the right in Fig. 7. The chattering in the control input contributes to faster fatigue of the robot mechanical parts and increases heating in the joint actuators. As such, the chattering may reduce the life span of the robot system and thus it should be avoided. The CPS of the control input depicted with the solid line implies that use of the Kalman filter helps in suppressing the chattering effects.

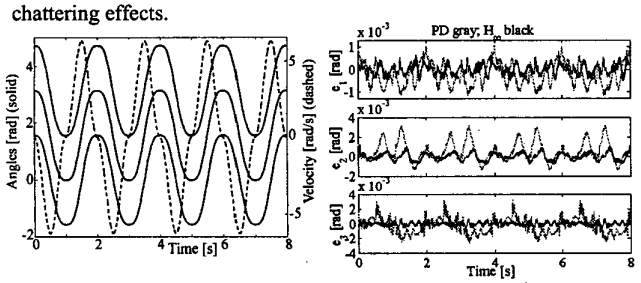

Fig. 6. Left: reference joint motions and velocity in the 1st experiment; right: achieved position errors in the joints

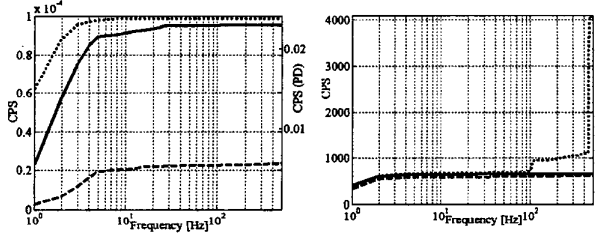

Fig. 7. CPS's of position error (left) and control input (right) for the 1st d.o.f. in the 1st experiment: dotted-PD without the filter (right scale), solid-PD with the filter, dashed-H_∞ (left scale)

Section IV explains how to design H_∞ controllers that satisfy specifications on the performance, but may also incorporate robustness against dynamic peculiarities recognized in the controlled plant. The controllers are calculated using the standard software routines [13] that require a parametric description of the plant model. Using an output error model structure with a least-square criterion, we may fit a parametric model (e.g., a transfer function) to the experimental data (solid line in Fig. 3). The frequency response function of the resulting model is depicted in Fig. 3 with the dashed line. The weighting functions, required for solving the MSP, are presented on the left in Fig. 8. They are formed in the disturbance-based control design cycles, with experiments within each iteration. Therefore, they account for the observed dynamic peculiarities of the robot. At low frequencies, $W_{1,1}(j\omega)$ (solid line) takes care about type k control, giving the useful suppression of the position errors within the bandwidth and strong rejection of low-frequent disturbances. It also aims at rejecting the parasitic effects around 13 Hz and 50 Hz. The former parasitic effect is due to the vibration of the base, already recognized at the beginning of this Section. The latter parasitic effect occurs at the anti-resonance frequency of the plant shown in Fig. 3. During the disturbance-based control design cycles an important contribution of this frequency to the tracking error was noticed. Therefore, the feedback controller is refined such to suppress effect of the parasitic frequency. Outside the bandwidth, the weighting function $W_{2,1}^{-1}(j\omega)$ (dashed line) accounts for the high-frequency roll-off and compensates effects of the resonance around 95 Hz. The compensator solving the MSP for the plant model shown in Fig. 3 and for the weightings depicted on the left in Fig. 8, are presented on the right-hand side in Fig. 8. When compared with the standard controllers depicted in Fig. 2, we may observe more involved shapes of both the magnitude and the phase plots, indicating a potential of this controller to simultaneously handle more versatile control objectives than the conventional ones. It is also worth noticing that the design of the H_∞ controller does not require an explicit treatment of the time-delay problem, which was the case with the conventional controller. It considers the delay as an inherent property of the controlled plant, and creates an optimal controller that handles this problem together with other control objectives.

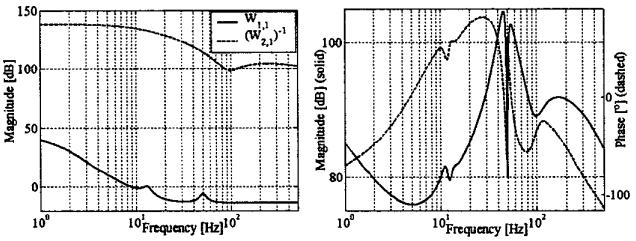

Fig. 8. Weigthing functions used for solving the MSP for the 1st d.o.f. (left) and the resulting H_∞ controller (right)

Simultaneous fulfillment of several control goals using the H_∞ controller becomes quite obvious from the Bode plots of the open-loop gain, presented in Fig. 4 with the dashed lines. Within the bandwidth, defined as the first zero-level crossing by the magnitude, the gain is much higher with the H_∞ controller than with the PD's. Outside the bandwidth, the H_∞ controller reduces the influence of the resonance around 95 Hz, and ensures decay at high-frequencies. A fair comparison between the effects of the conventional controller enhanced with the Kalman filter and the H_∞ controller also requires acknowledgement that the H_∞ controller has a slightly reduced phase margin around the cross-over frequency. As a direct consequence, we see from Fig. 5 that the corresponding sensitivity function has higher peaking around the cross-over than the sensitivity for the PD with the filter. Still, this peaking is the acceptable price we should pay to enjoy the benefits from the H_∞ controller. Within the bandwidth, sensitivity for the H_∞ controller is lower than for the conventional ones, implying a better reduction of the position errors. Peaking around 95 Hz is sufficiently reduced and that around 410 Hz vanishes. What is also important, the sensitivities shown in Fig. 5 correspond to the nominal plant model obtained from the type I identification experiment, that aim at averaging the robot dynamics resulting after application of the computed-torque controller. We are interested how robust the designed controller is for application within the complete configuration space of the robot. To investigate this, in Fig. 9 we plot the sensitivity from Fig. 5 together with a bunch of the sensitivity functions obtained for distinct static robot configurations, used in type II identification experiments. Observed differences between the sensitivity functions are small and acceptable, implying a robustifying property of the H_∞ controller.

When tested in the motion task defined on the left in Fig. 6, the H_∞ controller performs much better than the enhanced PD. This is sup-

ported by much smaller position errors in the robot joints, which are shown on the right in Fig. 8 with the black lines. It is particularly important that even for such demanding joint trajectories we can achieve an accurate tracking. CPS of the 1st error, shown on the left in Fig. 7 with the dashed line, reveals lower energy content compared with the PD cases. Since above the bandwidth of the joint references the CPS plot does not have abrupt changes in the slope, it appears that influence of disturbances on the trajectory tracking is eliminated. The chattering effect in the control input is also avoided, as obvious from the dashed plot on the right-hand side in Fig. 7.

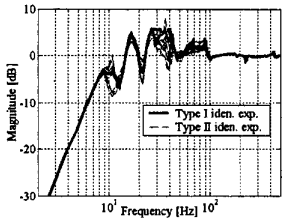

Fig. 9. Sensitivity functions for the 1st d.o.f. (H_∞ controller)

To additionally verify superior effects of the ES over the conventional control design, we carry out a second experiment in which the robot performs a writing task, often recognized as very demanding for the dynamics of a mechanical system [16]. The robot tip should write the sequence of letters shown on the left in Fig. 10. The letters lie in the vertical plane, parallel to the x_0z_0-surface (see Fig. 1). The corresponding joint motions are shown on the right in Fig. 10. Both PD with the filter and the H_∞ controllers were tested. Cartesian position errors are shown in Fig. 11. The H_∞ controller performs better than the conventional one along each direction. It achieves the errors (black lines) less than 1 mm, which is very accurate for a direct-drive robot.

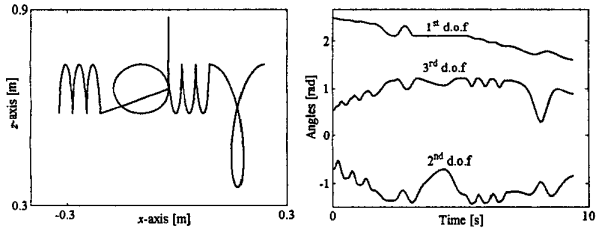

Fig. 10. Writing task as the 2nd experiment (left) and the related joint motions (right)

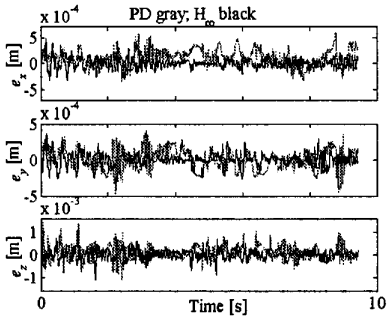

Fig. 11. Cartesian errors in the 2nd experiment

To the best of our knowledge, the presented errors are better than errors in compatible motion tasks, reported elsewhere in the literature. For example, they are much better than those presented in [6], although the control system used in [6] was running 2.5 times faster than ours. Frankly speaking, that system was implementing robust control algorithms allowing for high uncertainty in the nominal robot dynamic model. On the other hand, the motion tasks considered in that paper were less demanding than the tasks we adopt here, which privileges the quality of our results. Results presented in [5,7] correspond to even less challenging motion tasks, performed on geared robots. Even under such circumstances, the reported position errors are higher than those we can achieve.

VI. Conclusion

The motivation for the experimentally supported control design in robot motion control has been elaborated and supported by experimental results. It is true that such approach increases off-line design and tuning effort, but it also leads to successful achievement of the control specifications: high accuracy in tracking the reference joint trajectories from some prescribed frequency range, and the robustness against the modeling errors and disturbances. The experimentally supported design accounts for dynamic peculiarities (disturbances, flexibilities, noise) of the controlled plant. It is done via disturbance-based control design iterations. The resulting controllers are indeed specialized for the concrete robot, but they can significantly improve both the performance and the robustness properties, which is demonstrated on a challenging direct-drive robot.

References

[1] L. Sciavicco, B. Siciliano, *Modeling and Control of Robot Manipulators*, McGraw-Hill, London, 1996.

[2] J.J.E. Slotine, W. Li, *Applied Nonlinear Control*, Prentice Hall, London, 1991.

[3] Y. Chen, "Replacing a PID Controller by a Lag-Lead Compensator for a Robot–A Frequency Response Approach," *IEEE Trans. Rob. Autom.*, Vol. 5, No. 2, pp. 174-182, April 1989.

[4] B. de Jager, *Practical Evaluation of Robust Control for a Class of Nonlinear Mechanical Systems*, PhD Thesis, Eindhoven University of Technology, The Netherlands, 1992.

[5] H. Berghuis, H. Nijmeijer, "A Passivity Approach to Controller-Observer Design for Robots," *IEEE Trans. Rob. Autom.*, Vol. 9, No. 6, pp. 740-754, 1993.

[6] A. Jaritz, M.W. Spong, "An Experimental Comparison of Robust Control Algorithms on a Direct Drive Manipulator," *IEEE Trans. Control Sys. Tech.*, Vol. 4, No. 6, pp. 627-640, November 1996.

[7] H. Sage, et al., "Nonlinear Optimization of Robust H_∞ Controllers for Industrial Robot Manipulators," *Proc. IEEE Int. Conf. Rob. Autom.*, pp. 2352-2357, Albuquerque, New Mexico, April 1997.

[8] B. van Beek, B. de Jager, "RRR-Robot Design: Basic Outlines, Servo Sizing, and Control," *Proc. IEEE Int. Conf. Control Appl.*, pp. 36-41, Hartford, CT, 1997.

[9] M. Steinbuch, M.L. Norg, "Advanced Motion Control," *Europ. J. of Control*, Vol. 4, No. 4, pp. 278-293, 1998.

[10] P.R. Bélanger, et al, "Estimation of Angular Velocity and Acceleration from Shaft-Encoder Measurements," *Int. J. Rob. Res.*, Vol. 17, No. 11, pp. 1225-1233, November 1998.

[11] B. van Beek, B. de Jager, "An Experim. Facility for Nonlin. Robot Control," *Proc. IEEE Int. Conf. Control Appl.*, pp. 668-673, Hawai'i, 1999.

[12] H. Kwakernaak, "Robust Control and H_∞-optimization–Tutorial Paper," *Automatica*, Vol. 29, No. 2, pp. 255-273, 1993.

[13] G.J. Balas, et al., *μ-Analysis and Synth. Toolbox*, The Mathworks, 1998.

[14] D. Kostić, et al., "Modeling and Identification of an RRR-robot," *Proc. IEEE Conf. Dec. Control*, pp. 1144-1149, Orlando, FL, December 2001.

[15] D. Kostić, et al., "Closed-form Kinematic and Dynamic Models of an Industrial-like RRR Robot," *Proc. IEEE Conf. Rob. Automation*, pp. 1309-1314, Washington D.C., May 2002.

[16] V. Potkonjak, et al., "Concerning the Primary and Secondary Objectives in Robot Task Definition–The "Learn From Humans" Principle," *Math. and Comp. in Simul.*, Vol. 54, No. 1-3, pp. 145-157, 2000.